Nano Energy 33 (2017) 21–28

Contents lists available at ScienceDirect

Nano Energy

journal homepage: www.elsevier.com/locate/nanoen

Photo-assisted synthesis of zinc-iron layered double hydroxides/TiO_2 nanoarrays toward highly-efficient photoelectrochemical water splitting

Ruikang Zhang, Mingfei Shao*, Simin Xu, Fanyu Ning, Lei Zhou, Min Wei*

State Key Laboratory of Chemical Resource Engineering, Beijing Advanced Innovation Center for Soft Matter Science and Engineering, Beijing University of Chemical Technology, Beijing 100029, PR China

ARTICLE INFO

Keywords:
Photo-assisted electrodeposition
Core–shell nanowire arrays
Layered double hydroxides
Photoelectrochemical water splitting

ABSTRACT

A highly-matched semiconductor/cocatalyst is crucial to enhance the bulk charge separation and surface reaction kinetics of the photoelectrode in the solar water splitting system. In this work, well-aligned, hierarchical zinc-iron layered double hydroxide (LDH) is *in situ* synthesized on the surface of TiO_2 by a facile and effective photo-assisted electrodeposition (PED) method. An experimental-computational combination study reveals that the photogenerated holes of TiO_2 tend to travel to ZnFe-LDH which enhances the bulk charge separation; while ZnFe-LDH acts as a cocatalyst which accelerates the surface water oxidation reaction. The resulting TiO_2/ZnFe-LDH-PE photoanode exhibits a largely enhanced PEC performance: the photocurrent density at 1.0 V *vs.* RHE is 2.29 and 1.31 times higher than that of the pristine TiO_2 and TiO_2/ZnFe-LDH-E (prepared by a conventional electrosynthesis method) photoanode, with 150 mV and 50 mV of negative shift for onset potential. This can be ascribed to the enhanced interface interaction and highly-matched band structure between ZnFe-LDH and TiO_2. It is expected that this strategy can be extended to other heterostructures for advanced performance in the fields of energy conversion and storage.

1. Introduction

Photoelectrochemical (PEC) water splitting has been recognized as one of the most promising technologies to provide clean, cost-effective hydrogen fuel with a high solar-to-chemical energy conversion [1–4]. Particularly, photoanode plays a key role in the PEC water splitting system due to the multistep proton-coupled electron transfer in water oxidation. Although semiconductors (*e.g.*, TiO_2 [5–7], α-Fe_2O_3 [8–10], WO_3 [11–13] and $BiVO_4$ [14–16]) have been extensively studied as photoanodes for water splitting, they normally suffer from poor holes transfer efficiency and slow surface oxidation reaction. To address these limitations, an efficient technique is to introduce oxygen evolution reaction (OER) cocatalysts to collaborate with semiconductors, which would improve the activity of photoanode by reducing the overpotential of water oxidation [17–21]. Unfortunately, the as-formed semiconductor/cocatalysts (sem/cat) interface inevitably generates new electron-hole recombination centers, resulting in degradation of PEC water splitting performance.

Aiming at “adaptive-interface” in the heterostructure of photoanodes, great efforts have been developed by either constructing nanostructures to minimize charge transfer distance or modifying cocatalysts to enhance hole transfer efficiency [22–25]. Practically, the establishment of an optimized buried junction with conductive and chemically stable surface is essential for the deposition of cocatalysts. Recently, a uniform cocatalyst film over the semiconductor has been reported by using photo-assisted deposition strategy, which has shown largely enhanced PEC water splitting performance [26]. As a class of 2D structure anionic clays, layered double hydroxides (LDHs) have attracted increasing attention owing to their tunable chemical composition and multi-functionalities [27–30]. Especially, the transition metal-containing LDHs have shown highly-efficient catalytic performance toward electrochemical water splitting, which can be used as cocatalysts in PEC water splitting. In our previous work, the *in situ* electrodeposition of layered double hydroxide (LDHs) nanoplatelets arrays on the surface of semiconductor core has been demonstrated as an efficient way to construct sem/cat photoanode [31,32]. In despite of some progresses, how to design and fabricate photoanodes with highly-matched sem/cat interface through material design and synthesis exploration remains a big challenge.

Herein, we report the fabrication of well-aligned TiO_2/ZnFe-LDH hierarchical nanoarrays (NAs) by direct deposition of ZnFe-LDH nanosheets on TiO_2 NAs *via* a photo-assisted electrodeposition (PED) method (denoted as TiO_2/ZnFe-LDH-PE). In comparison with the counterpart material prepared by a pristine electrodeposition (ED)

* Corresponding authors.
E-mail addresses: shaomf@mail.buct.edu.cn (M. Shao), weimin@mail.buct.edu.cn (M. Wei).

http://dx.doi.org/10.1016/j.nanoen.2017.01.020
Received 3 October 2016; Received in revised form 9 January 2017; Accepted 9 January 2017
Available online 10 January 2017

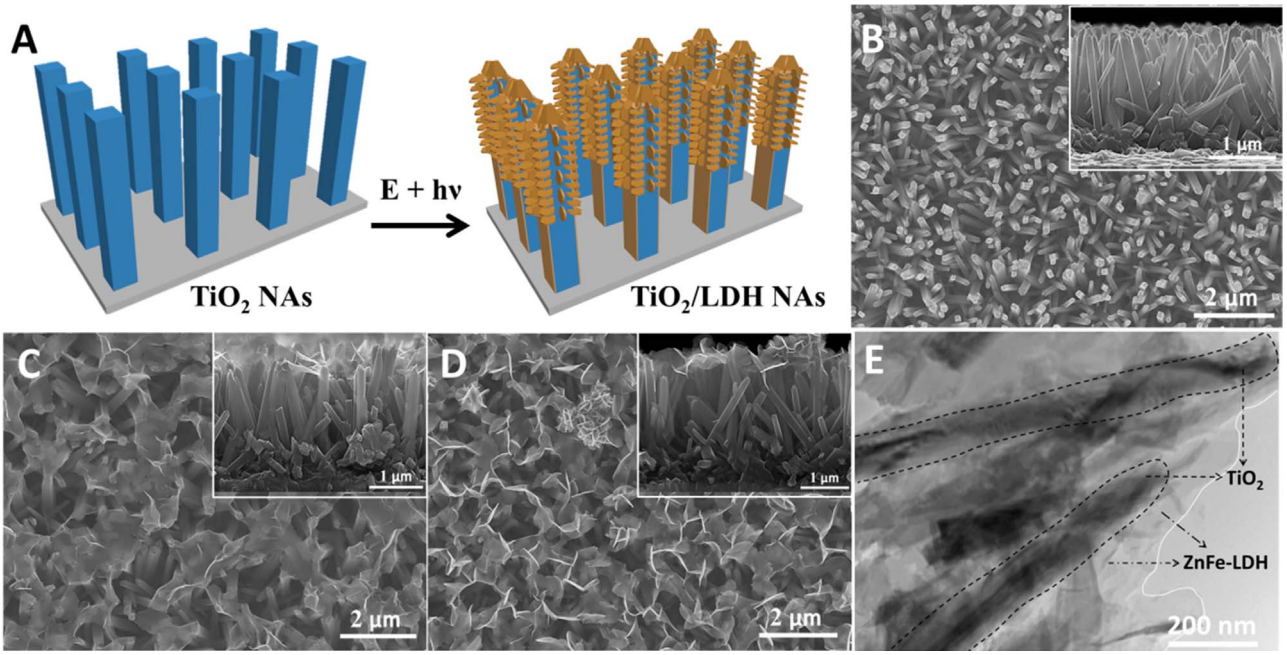

Fig. 1. (A) Schematic illustration for the fabrication of TiO_2/ZnFe-LDH-PE NAs. SEM images of (B) TiO_2, (C) TiO_2/ZnFe-LDH-E and (D) TiO_2/ZnFe-LDH-PE NAs, respectively. (E) TEM image of TiO_2/ZnFe-LDH-PE NAs.

method (denoted as TiO_2/ZnFe-LDH-E), the TiO_2/ZnFe-LDH-PE sample shows significantly improved charge separation and hole injection efficiency, which is attributed to the strongly-bound sem/cat interface. As a result, the TiO_2/ZnFe-LDH-PE NAs sample gives a largely enhanced PEC performance: the photocurrent density at 1.0 V *vs.* RHE is 1.31 and 2.29 times higher than that of TiO_2/ZnFe-LDH-E NAs and pristine TiO_2 NAs, respectively, with 50 mV and 150 mV of negative shift for onset potential. A combination study based on experiment and density functional theory (DFT) calculation reveals that the photo-induced holes tend to transfer from TiO_2 to ZnFe-LDH due to the matched band structure, which is essential to accelerate the water oxidation.

2. Experimental sections

2.1. Preparation of TiO_2/ZnFe-LDH-PE and TiO_2/ZnFe-LDH-E NAs

The TiO_2 NAs was prepared on FTO substrate using a previously reported hydrothermal method [33]. Photo-assisted electrodeposition of ZnFe-LDH was performed in a three-electrode configuration by using TiO_2 NAs as working electrode, Pt wire as counter electrode, and saturated calomel electrode (SCE) as reference electrode. The electrolyte was obtained by dissolving $Zn(NO_3)_2{\cdot}6H_2O$ (0.1 M) and $FeCl_2{\cdot}6H_2O$ (0.15 M) in 50 mL of distilled water, which was agitated by a magnetic stirrer with a continuous N_2 flow to prevent the oxidation of Fe^{2+}. The potentiostatic deposition was carried out at a potential of −1.0 V *vs.* SCE with light illumination at a power density of 100 mW cm^{-2} by a 150 W Xe lamp. The resulting hierarchical NAs sample was withdrawn and rinsed with distilled water, and then was placed in ambient air for the self-oxidation of Fe^{2+} to Fe^{3+}(denoted as TiO_2/ZnFe-LDH-PE). The electrodeposition of ZnFe-LDH onto TiO_2 NWs was performed by the same method but without the illumination (denoted as TiO_2/ZnFe-LDH-E).

2.2. Characterizations

The morphology was investigated using a scanning electron microscopy (SEM; Zeiss SUPRA 55) with an accelerating voltage of 20 kV combined with energy dispersive X-ray (EDX) spectroscopy. Transmission electron microscopy (TEM) images were recorded using a Hitachi H-800 TEM with an accelerating voltage of 200 kV. X-ray diffraction (XRD) patterns were collected on a Rigaku XRD-6000 diffractormeter using Cu Kα radiation. Solid UV–vis diffuse reflection spectra were collected on a Shimadzu U-3000 spectrophotometer. Fluorescence spectra were recorded on a RF-5301PC fluorospectrophotometer with an excitation wavelength of 300 nm. X-ray photoelectron spectra (XPS) were performed on a Thermo VG ESCALAB 250 X-ray photoelectron spectrometer using Al Kα radiation at a pressure of about 2×10^{-9} Pa.

2.3. Photoelectrochemical measurements

All the PEC water splitting performances were operated on an electrochemical workstation (CHI 660e, CH Instruments Inc., Shanghai) at room temperature in a neutral medium of a 0.5 M Na_2SO_4 aqueous solution with a conventional three-electrode cell. Illumination source was a 150 W Xe lamp with a power density of 100 mW cm^{-2}. The as-obtained TiO_2, TiO_2/ZnFe-LDH-E and TiO_2/ZnFe-LDH-PE NAs on FTO substrate as working electrode were immersed in the electrolyte with an area of 1 cm×3 cm. The working, counter (a Pt wire), and reference (a saturated calomel electrode (SCE)) electrode are installed in a quartz cell. The photocurrent was measured by cyclic voltammetry (CV) or linear sweep voltammetry (LSV) at a scan rate of 10 mV s^{-1}. For the incident photon to current efficiency (IPCE) tests, the photocurrent was measured by LSV under monochromatic light irradiation by using optical filter on the Xe lamp (see details in the Supporting information). Electrochemical impedance spectroscopy (EIS) was carried out by applying an AC voltage at 0 V with frequency ranging from 100 kHz to 0.01 Hz under illumination. Mott-Schottky plots were evaluated at DC potential range from −1.0 to 0.4 V at a frequency of 1 kHz. The photoelectrochemically generated gas was collected in a home-made airtight transparent electrochemical cell by a drainage method.

3. Results and discussion

3.1. Materials preparation and characterization

The preparation process of TiO_2/ZnFe-LDH-PE photoelectrode is illustrated in Fig. 1A, which involves the photo-assisted electrodeposition of ZnFe-LDH nanoplatelets onto the TiO_2 nanoarrays (NAs). Typically, vertically-aligned TiO_2 NAs was firstly grown on the fluorine-doped tin oxide (FTO) substrate *via* a hydrothermal method as described previously [33], with an average diameter of ~100 nm and an average length of ~2.0 μm (Fig. 1B). The ZnFe-LDH was *in situ* synthesized on the surface of TiO_2 NAs by using electrochemical method with a Xe lamp illumination. Compared with TiO_2/ZnFe-LDH-E prepared by a pristine electrosynthesis method, the LDH nanoplatelets are more uniformly dispersed in the TiO_2/ZnFe-LDH-PE electrode with well-defined plate-like morphology, suggesting the illumination facilitates the crystallization/evolution of LDH nanoplatelets on the surface of TiO_2 NAs (Fig. 1C and D). The TEM image shows a core-shell hierarchical nanostructure of TiO_2/ZnFe-LDH-PE NAs (Fig. 1E), which is consist with the SEM images. It is worth mention that the ZnFe-LDH nanoplatelets are mainly deposited on the upper-half of TiO_2 NAs, with a low density on the bottom part (Fig. S1). The molar ratio of Zn/Fe in TiO_2/ZnFe-LDH-E and TiO_2/ZnFe-LDH-PE is close based on energy dispersive X-ray (EDX) spectroscopy (Fig. S2), implying that the PED method does not affect the chemical composition of introduced ZnFe-LDH. It is found that a higher illumination power density leads to a more uniform dispersion of ZnFe-LDH nanoplatelets (Fig. S3). The influence of deposition time (from 25 s to 200 s) on the production of TiO_2/ZnFe-LDH-E and TiO_2/ZnFe-LDH-PE were also carried out (Fig. S4–S6). After 50 s of electrodeposition, a more dense packing of ZnFe-LDH in TiO_2/ZnFe-LDH-PE is observed than that in TiO_2/ZnFe-LDH-E (Zn/Fe/Ti ratio: 0.26/0.81/32.43 *vs.* 0.18/0.56/32.42). As the deposition time increases, a thin LDH layer with plate-like morphology appears on the surface of TiO_2 NWs, without obvious distinction between these two group samples. This indicates that the illumination imposes influence on the crystallization of ZnFe-LDH but has little effect on the following crystal growth process.

XRD patterns of TiO_2, TiO_2/ZnFe-LDH-E and TiO_2/ZnFe-LDH-PE are shown in Fig. 2A, from which two sharp reflections located at 36.1° and 62.8° are observed for all these three samples, corresponding to the (101) and (002) diffraction peak of rutile TiO_2 (JCPDS No. 21-1276), respectively. For the latter two samples, the (003) reflection of a typical LDH phase at 11.6° appear, indicating the successful synthesis of ZnFe-LDH on the surface of TiO_2 NAs. The stronger intensity of (003) reflection in TiO_2/ZnFe-LDH-PE relative to TiO_2/ZnFe-LDH-E suggests a higher crystalline degree of ZnFe-LDH, which is in accordance with the result of SEM observations. In addition, a prolonged deposition time induces an enhancement in the intensity of (003) reflection for LDH (Fig. S7).

X-ray photoelectron spectroscopy (XPS) was performed to explore the effect of illumination on the heterostructure of ZnFe-LDH and TiO_2. Fig. 2B shows the Ti 2p XPS spectra for TiO_2, TiO_2/ZnFe-LDH-E and TiO_2/ZnFe-LDH-PE NAs. The pure TiO_2 NAs display two peaks at 458.6 and 464.3 eV, corresponding to Ti $2p_{3/2}$ and Ti $2p_{1/2}$, respectively [34]. After the deposition of ZnFe-LDH, both the two peaks shift to lower energy level, suggesting the electron transfer from ZnFe-LDH to TiO_2. A larger shift (0.4 eV) of Ti $2p_{3/2}$ for TiO_2/ZnFe-LDH-PE compared with TiO_2/ZnFe-LDH-E (0.3 eV) is observed, indicating a stronger interaction between TiO_2 and ZnFe-LDH obtained by the PED method. Fig. 2C and D show the Zn 2p and Fe 2p XPS spectra for the three samples. Compared with the pure ZnFe-LDH, an obvious positive shift in Zn 2p peaks and a slight positive shift in Fe 2p peaks are observed for TiO_2/ZnFe-LDH-E and TiO_2/ZnFe-LDH-PE, confirming the electron transfer from ZnFe-LDH to TiO_2. Similarly, a larger shift (0.35 eV) of Zn $2p_{3/2}$ for TiO_2/ZnFe-LDH-PE relative to TiO_2/ZnFe-LDH-E (0.20 eV) further verifies a stronger electron interaction between TiO_2 and PE-deposited ZnFe-LDH. As a result, the photo-assisted electrodeposition leads to a high crystallinity of ZnFe-LDH on the surface of TiO_2 NAs with an enhanced electron transfer. A strong interface interaction between photocatalyst and cocatalyst would influence the resulting PEC properties, which will be discussed in the next section.

3.2. Studies on PEC water splitting

PEC water splitting measurements were subsequently carried out for the three samples in a neutral medium (0.5 M Na_2SO_4 aqueous solution). As shown in Fig. 3A, pristine TiO_2 NAs display a relatively low photoresponse with a photocurrent density of 0.79 mA cm^{-2} at 1.23 V *vs.* RHE. A largely enhanced photocurrent density (1.26 mA cm^{-2}) is observed for the TiO_2/ZnFe-LDH-E NAs. In the case of TiO_2/ZnFe-LDH-PE NAs, the photocurrent density further reaches to 1.51 mA cm^{-2} at 1.23 V *vs.* RHE, 1.91 and 1.20 times higher than that of the pristine TiO_2 and TiO_2/ZnFe-LDH-E NAs samples, respectively. The onset potential of TiO_2/ZnFe-LDH-PE NAs also has an obvious negative shift compared with the other two samples. In addition, transient photocurrent measurements were carried out under chopped light illumination (Fig. 3B). All these samples display a prompt and reproducible photocurrent response with respect to the ON-OFF cycles of the irradiation signal, which further demonstrates the improvement in PEC performance by the PE-deposited ZnFe-LDH. Moreover, the photoconversion efficiency of each photoanode (Fig. 3C) was calculated based on the current-voltage (J-V) curve as a function of applied voltage, giving the following order: TiO_2/ZnFe-LDH-PE > TiO_2/ZnFe-LDH-E > TiO_2 NAs. Incident photon to current efficiency (IPCE) results show that all these samples exhibit photocatalytic activity in UV region (below 420 nm) and inactivity in the visible region (Fig. 3D), which suggests TiO_2 serves as photocatalyst for the generation of electron and hole. The TiO_2/ZnFe-LDH-PE photoanode shows the highest IPCE at 400 nm: 4.86% *vs.* 2.50% and 4.61% for TiO_2 and TiO_2/ZnFe-LDH-E. The faradaic efficiency is obtained by comparing the theoretical O_2 production calculated from the photocurrent with the actual gas yield (Fig. 3E and Fig. S8). In three cycles, TiO_2/ZnFe-LDH-PE photoanode gives an average O_2 production of 15.15 μmol h^{-1}, which is 1.77 and 1.13 times higher than that of TiO_2 and TiO_2/ZnFe-LDH-E photoanode, respectively. The photocurrent-to-oxygen conversion efficiencies for the three samples are nearly 100%, indicating the increased photocurrent is due to water oxidation. A durability test based on chronoamperometric measurements shows that all the three samples give a stable photocurrent (< 5% current decay) under irradiation for 10 h (Fig. 3F). For the used TiO_2/ZnFe-LDH-PE photoanode after durability tests, the ZnFe-LDH nanoplatelets maintain their original hierarchical architecture (Fig. S9). In addition, the pure ZnFe-LDH on FTO shows a slight photoresponse under illumination, further illustrating that TiO_2 serves as semiconductor to generate electrons and holes in the composite photoanode (Fig. S10). The results above demonstrate that the introduction of ZnFe-LDH by the PED method enhances the PEC properties of the as-obtained TiO_2/ZnFe-LDH-PE photoanode.

Furthermore, the PEC water splitting performances of TiO_2/ZnFe-LDH-PE photoanode with various illumination power density or deposition time were investigated. The LSV curves for the five TiO_2/ZnFe-LDH-PE samples prepared with different illumination power density (from 0 to 150 mW cm^{-2}) are shown in Fig. 4A. The photocurrent density enhances along with increased illumination power density from 0 to 100 mW cm^{-2}, and shows no further change from 100 to 150 mW cm^{-2}, which suggests that the photo-assisted deposi-

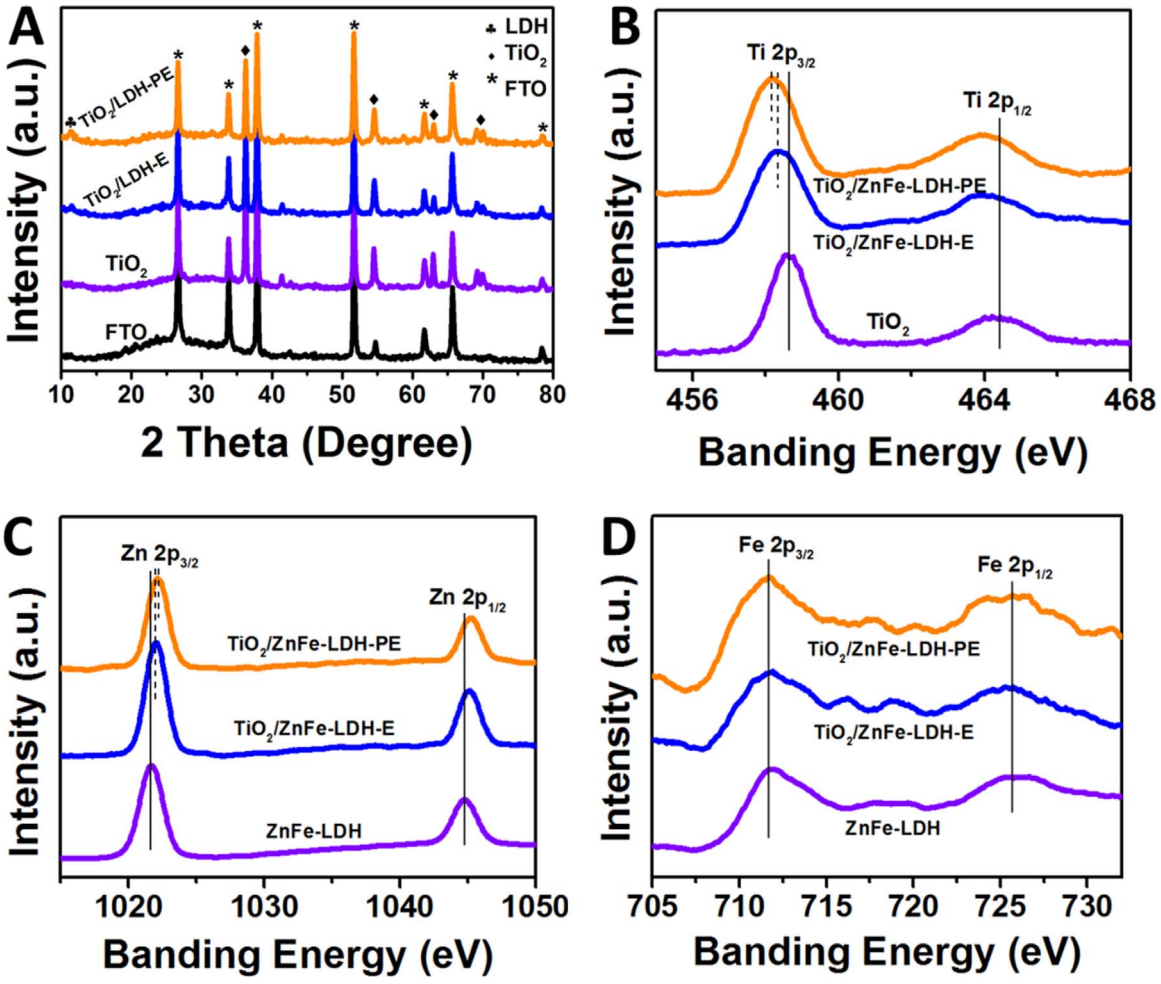

Fig. 2. (A) XRD patterns of FTO substrate, TiO_2, TiO_2/ZnFe-LDH-E and TiO_2/ZnFe-LDH-PE NAs, respectively. (B) Ti 2p XPS spectra of TiO_2, TiO_2/ZnFe-LDH-E and TiO_2/ZnFe-LDH-PE NAs, respectively. (C) Zn 2p and (D) Fe 2p XPS spectra of ZnFe-LDH, TiO_2/ZnFe-LDH-E and TiO_2/ZnFe-LDH-PE NAs, respectively.

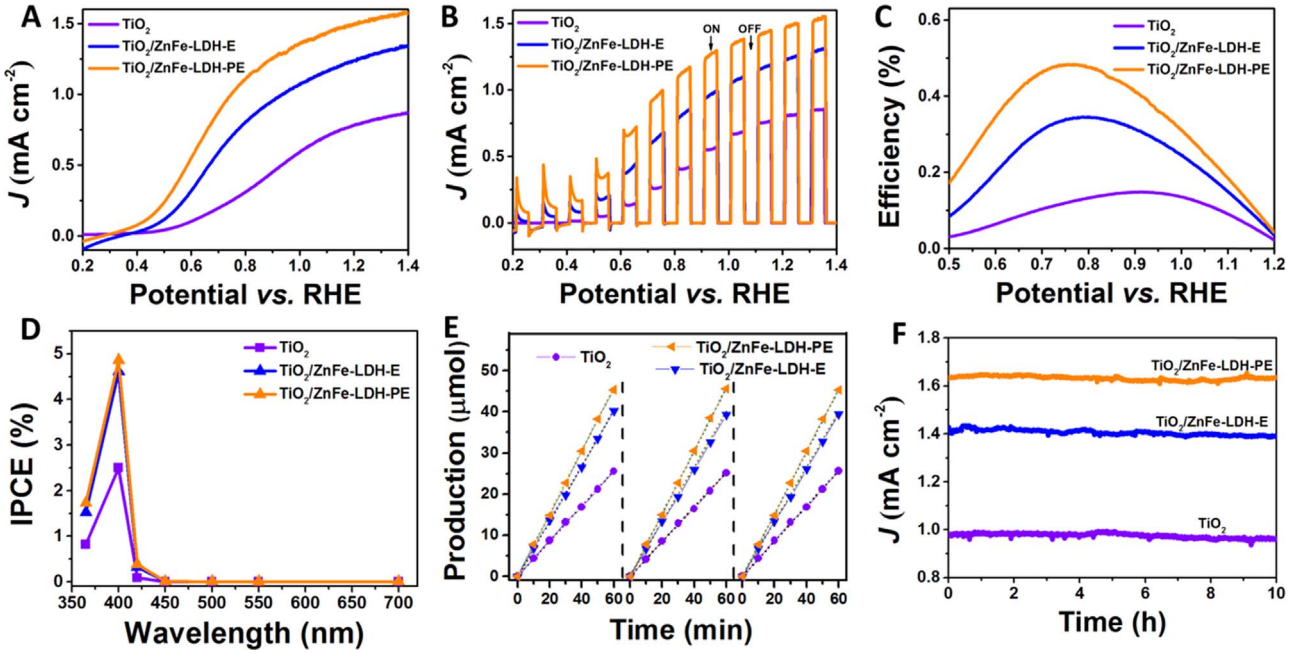

Fig. 3. (A) *J*-V curves, (B) *J*-V behavior under chopped light illumination; (C) the calculated photoconversion efficiency as a function of applied voltage; (D) IPCEs measured at 1.23 V *vs.* RHE, (E) total O_2 production detected by a gas chromatograph in three cycles (the dash line represents the theoretic O_2 production calculated from the measured photocurrent); (F) the steady-state photocurrent at 0.6 V *vs.* SCE for the samples of TiO_2, TiO_2/ZnFe-LDH-E and TiO_2/ZnFe-LDH-PE photoanodes, respectively.

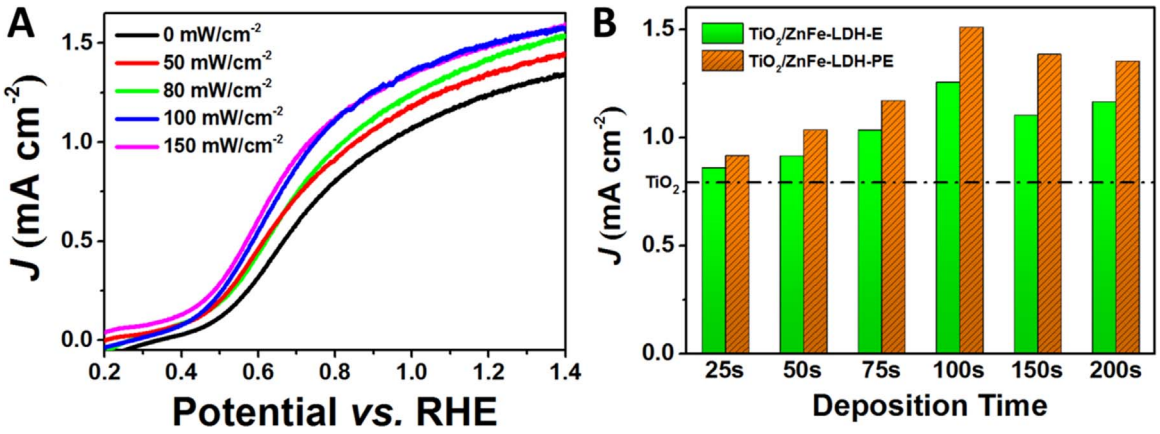

Fig. 4. (A) *J*-V curves for the five TiO_2/ZnFe-LDH-PE samples prepared with various illumination intensity (0, 50, 80, 100,150 mW cm^{-2}); (B) photocurrent density at 1.23 V *vs.* RHE for the samples of TiO_2/ZnFe-LDH-E and TiO_2/ZnFe-LDH-PE with various deposition time (25 s, 50 s, 75 s, 100 s, 150 s, 200 s), respectively.

tion of ZnFe-LDH plays a vital role in the improvement of PEC performance. The effect of LDHs deposition time is also studied (Fig. 4B and Fig. S11): the photocurrent of TiO_2/ZnFe-LDH increases firstly and then decreases along with the increase of LDH deposition time, and the maximum photocurrent density (1.51 mA cm^{-2} at 1.23 V *vs.* RHE) is obtained for the TiO_2/ZnFe-LDH (100 s) sample. This indicates that the coating of LDH onto TiO_2 at a suitable level can effectively enhance the photocatalytic activity of TiO_2; an excess of LDH incorporation with a dense packing would hinder the charge transfer. In addition, all the TiO_2/ZnFe-LDH-PE samples exhibit a higher photocurrent density than that of corresponding TiO_2/ZnFe-LDH-E ones with the same LDH deposition time, demonstrating the superiority of the photo-assisted electrodeposition method.

3.3. Mechanism discussion

To give a deep insight into the largely enhanced PEC water splitting performance of TiO_2/ZnFe-LDH-PE NAs, the optical properties of the three typical samples were investigated by UV–vis diffuse reflectance spectroscopy and photoluminescence (PL) emission spectra. The absorption in the UV light region nearly remains the same after the introduction of ZnFe-LDH by the two methods (Fig. 5A). A slightly enhanced absorption in 400–450 nm is observed in the TiO_2/ZnFe-LDH-E and TiO_2/ZnFe-LDH-PE sample, originating from the visible light response of ZnFe-LDH [35]. However, the rather low IPCE (Fig. 3D) in visible region indicates that TiO_2 acts as the predominant light responsive photocatalyst. The PL behavior, originating from the recombination of photoinduced electron-hole pair, can reflect the surface separation efficiency of charge carriers in semiconductors. As shown in Fig. 5B, pure TiO_2 NAs display rather strong PL emission peaks within 410–490 nm region, which are attributed to the band gap transition and the charge transfer transition of oxygen vacancy trapped electrons [36]. In contrast, the PL intensity of TiO_2/ZnFe-LDH-E decreases significantly, and the TiO_2/ZnFe-LDH-PE sample gives a further decline, which indicates a suppressed recombination of photo-generated charge carriers with the incorporation of ZnFe-LDH.

The charge separation efficiency and surface charge injection efficiency are usually used to quantify charge separation property and surface reaction kinetics (see details in the experimental section, Fig. S12) [32,37,38]. For the sample of TiO_2/ZnFe-LDH-PE, the charge separation efficiency is calculated to be 99.1% at 1.23 V *vs.* RHE (Fig. 5C), much larger than that of pristine TiO_2 (65.3%) and TiO_2/ZnFe-LDH-E (87.6%) NAs. The charge injection efficiency at 1.23 V *vs.* RHE is 62.6%, 80.4% and 88.7% for TiO_2, TiO_2/ZnFe-LDH-E and TiO_2/ZnFe-LDH-PE sample, respectively (Fig. 5 D). This indicates that the charge transfer is greatly accelerated and the water oxidation is facilitated in TiO_2/ZnFe-LDH-PE NAs. The electrochemical impedance spectroscopy (EIS) curves of the three samples are shown in Fig. 5E. As reported, the first arc (high frequency) represents the charge transfer step and the second arc (low frequency) corresponds to the surface water oxidation step [6]. After the incorporation of ZnFe-LDH, the diameter of both two arcs decreases significantly, indicating ZnFe-LDH can enhance the charge separation and charge injection efficiency of TiO_2 simultaneously. Moreover, the TiO_2/ZnFe-LDH-PE shows a more obvious enhancement effect, in agreement with the results of charge separation and surface charge injection efficiency. The positive slopes of the Mott-Schottky plots (Fig. 5F) for all these samples indicate the n-type TiO_2 semiconductor as expected [39]. The flat band potential (E_{FB}) value and the charge carrier density can be calculated according to the Mott-Schottky equation (see experimental sections for details). The charge carrier density is 2.48×10^{16}, 3.94×10^{16} and 4.61×10^{16} cm^{-3} for TiO_2, TiO_2/ZnFe-LDH-E and TiO_2/ZnFe-LDH-PE, respectively. This demonstrates an enhanced carrier density on the surface, which is more significant in the case of TiO_2/ZnFe-LDH-PE sample. The result can partly be validated by the PL emission spectra (Fig. 5B). A positive shift of flat band potential for the two TiO_2/ZnFe-LDH samples suggests a decrease in the bending of band edge, which can be attributed to the facilitated electrode/electrolyte interface charge transfer.

To further reveal the synergistic effect between ZnFe-LDH and TiO_2 on the improvement of PEC performance, the density functional theory plus U (DFT + U) method was employed to calculate the band edge placement of each component in TiO_2/ZnFe-LDH. The detailed information of model construction and computational method is described in the Supporting information (Computational Details and Fig. S13–S15). The average distance between the terminal oxygen atom in TiO_2 surface and the hydrogen atom in ZnFe-LDH surface is only 2.27 Å (Fig. 6A); and the binding energy between them is −9.96 eV. The work function and band gap energy of TiO_2 are calculated to be 5.651 eV and 3.031 eV (Fig. S14). Accordingly, the CBM and VBM of TiO_2 are determined to be −4.136 eV and −7.167 eV relative to vacuum level, respectively. By the same method, the work function and band gap energy of ZnFe-LDH are calculated to be 4.485 eV and 2.114 eV (Fig. S15), which is basically consist with the reported results [40]. The CBM and VBM of ZnFe-LDH are located at −3.428 eV and −5.542 eV *vs.* vacuum level, respectively. Given the calculation above, a mechanism for the enhanced PEC water oxidation performance in the TiO_2/ZnFe-LDH system is proposed (Fig. 6B). The electron-hole pair is firstly generated in TiO_2 under illumination; and the photogenerated holes on the valence band of TiO_2 tend to travel to ZnFe-LDH. The

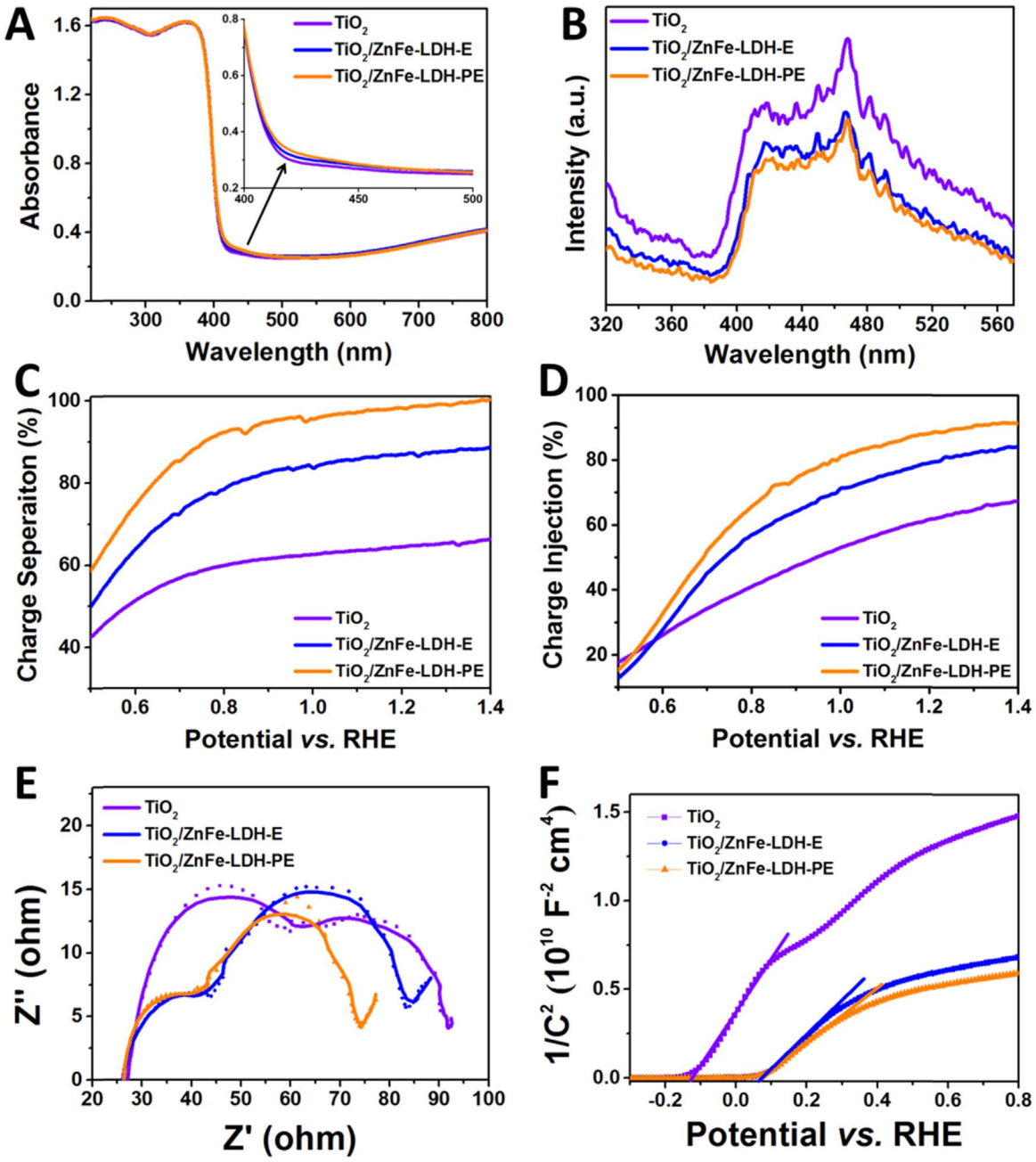

Fig. 5. (A) UV–vis diffuse-reflectance spectra, (B) PL spectra, (C) charge separation efficiency and (D) charge injection efficiency *vs.* potential curves, (E) EIS measured at 0 V *vs.* SCE under illumination, (F) Mott-Schottky plots collected at a frequency of 1 kHz in dark for the samples of TiO_2, TiO_2/ZnFe-LDH-E and TiO_2/ZnFe-LDH-PE, respectively.

electrons of ZnFe-LDH migrate to the current collector through TiO_2 NAs due to the electric potential difference. This electron-hole transfer based on the energy difference of band edge position shows a high accordance with the XPS results. On the other hand, holes are captured by ZnFe-LDH along with the oxidation of Fe, which acts as the active site for water oxidation [24,41]. For the TiO_2/ZnFe-LDH-PE NAs, the charge separation efficiency enhances more prominently (Fig. 5C and E), resulting from a stronger interface interaction between ZnFe-LDH and TiO_2 (Fig. 2). In addition, a more uniform dispersion of ZnFe-LDH in TiO_2/ZnFe-LDH-PE contributes to the enhancement of water oxidation efficiency. Therefore, the TiO_2/LDH heterostructure prepared by the photo-assisted strategy exhibits an excellent PEC water splitting performance.

4. Conclusions

In summary, well-aligned, hierarchical TiO_2/ZnFe-LDH NAs have been successfully fabricated by a facile and effective PED method. The resulting TiO_2/ZnFe-LDH-PE photoanode exhibits largely enhanced PEC water splitting performance compared with the TiO_2/ZnFe-LDH-E and pristine TiO_2 NWs, owing to the improved charge separation and injection efficiency. This is ascribed to the enhanced interface interaction and highly-matched band structure between ZnFe-LDH and TiO_2. It is expected that this strategy can be extended to other heterostructures for advanced performance in the fields of energy conversion and storage.

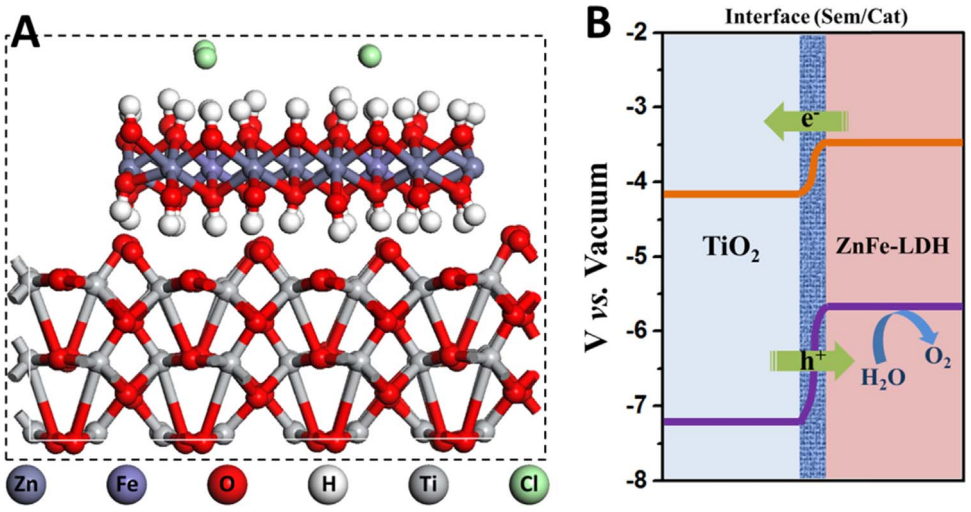

Fig. 6. (A) Optimized geometry of TiO_2/ZnFe-LDH model; (B) a schematic illustration for the PEC water oxidation process over the TiO_2/ZnFe-LDH photoanode.

Acknowledgements

This work was supported by the National Natural Science Foundation of China (No. U1462118), the 973 Program (No. 2014CB932102), and the Fundamental Research Funds for the Central Universities (buctrc201506).

Appendix A. Supplementary material

Supplementary data associated with this article can be found in the online version at http://dx.doi.org/10.1016/j.nanoen.2017.01.020.

References

[1] M. Grätzel, Nature 414 (2001) 338–344.
[2] P. Du, R. Eisenberg, Energy Environ. Sci. 5 (2012) 6012–6021.
[3] F.E. Osterloh, Chem. Soc. Rev. 42 (2013) 2294–2320.
[4] S. Cao, X. Yan, Z. Kang, Q. Liang, X. Liao, Y. Zhang, Nano Energy 24 (2016) 25–31.
[5] G. Wang, H. Wang, Y. Ling, Y. Tang, X. Yang, R.C. Fitzmorris, C. Wang, J. Zhang, Y. Li, Nano Lett. 11 (2011) 3026–3033.
[6] P. Yan, G. Liu, C. Ding, H. Han, J. Shi, Y. Gan, C. Li, ACS Appl. Mater. Interfaces 7 (2015) 3791–3796.
[7] X. Wang, R. Long, D. Liu, D. Yang, C. Wang, Y. Xiong, Nano Energy 24 (2016) 87–93.
[8] D. Qin, C. Tao, S. In, Z. Yang, T.E. Mallouk, N. Bao, C.A. Grimes, Energy Fuels 25 (2011) 5257–5263.
[9] Y. Ling, G. Wang, D.A. Wheeler, J. Zhang, Y. Li, Nano Lett. 11 (2011) 2119–2125.
[10] P. Dias, A. Vilanova, T. Lopes, L. Andrade, A. Mendes, Nano Energy 23 (2016) 70–79.
[11] J. Zhang, X. Wang, X. Xia, C. Gu, J. Tu, Sol. Energy Mater. Sol. Cells 95 (2011) 2107–2112.
[12] S. Wang, H. Chen, G. Gao, T. Butburee, M. Lyu, S. Thaweesak, J. Yun, A. Du, G. Liu, L. Wang, Nano Energy 24 (2016) 94–102.
[13] J. Zhang, P. Zhang, T. Wang, J. Gong, Nano Energy 11 (2015) 189–195.
[14] A. Iwase, A. Kudo, J. Mater. Chem. 20 (2010) 7536–7542.
[15] Y. Ng, A. Iwase, A. Kudo, R. Amal, J. Phys. Chem. Lett. 1 (2010) 2607–2612.
[16] Q. Jia, K. Iwashina, A. Kudo, PANS 109 (2012) 11564–11569.
[17] D.K. Zhong, D.R. Gamelin, J. Am. Chem. Soc. 132 (2010) 4202–4207.
[18] Y. Hou, X. Li, Q. Zhao, X. Quan, G. Chen, Adv. Funct. Mater. 20 (2010) 2165–2174.
[19] J.A. Seabold, K.S. Choi, Chem. Mater. 23 (2011) 1105–1112.
[20] W. Li, S.W. Sheehan, D. He, Y. He, X. Yao, R.L. Grimm, G.W. Brudvig, D. Wang, Angew. Chem. Int. Ed. 54 (2015) 11428–11432.
[21] X. Zheng, C. Dinh, F.P.G. de Arquer, B. Zhang, M. Liu, O. Voznyy, Y. Li, G. Knight, S. Hoogland, Z. Lu, X. Du, E. Sargent, Small 12 (2016) 3181–3188.
[22] J. Zhang, J. Bang, C. Tang, P.V. Kamat, ACS Nano 4 (2010) 387–395.
[23] P. Rao, L. Cai, C. Liu, I. Cho, C.H. Lee, J.M. Weisse, P. Yang, X. Zheng, Nano Lett. 14 (2014) 1099–1105.
[24] B.M. Klepser, B.M. Bartlett, J. Am. Chem. Soc. 136 (2014) 1694–1697.
[25] G.M. Carroll, D.K. Zhong, D.R. Gamelin, Energy Environ. Sci. 8 (2015) 577–584.
[26] D.K. Zhong, M. Cornuz, K. Sivula, M. Grätzel, D.R. Gamelin, Energy Environ. Sci. 4 (2011) 1759–1764.
[27] Q. Wang, D. O'Hare, Chem. Rev. 112 (2012) 4124–4155.
[28] Q. Wang, H. Tay, Z. Zhong, J. Luo, A. Borgna, Energy Environ. Sci. 5 (2012) 7526–7530.
[29] M. Shao, R. Zhang, Z. Li, M. Wei, D.G. Evans, X. Duan, Chem. Commun. 51 (2015) 15880–15893.
[30] C. Tang, H. Wang, H. Wang, Q. Zhang, G. Tian, J. Nie, F. Wei, Adv. Mater. 27 (2015) 4516–4522.
[31] M. Shao, F. Ning, M. Wei, D.G. Evans, X. Duan, Adv. Funct. Mater. 24 (2014) 580–586.
[32] F. Ning, M. Shao, S. Xu, Y. Fu, R. Zhang, M. Wei, D.G. Evans, X. Duan, Energy Environ. Sci. 9 (2016) 2633–2643.
[33] B. Liu, E.S. Aydil, J. Am. Chem. Soc. 131 (2009) 3985–3990.
[34] W. Ren, Z. Ai, F. Jia, L. Zhang, X. Fan, Z. Zou, Appl. Catal. B 69 (2007) 138–144.
[35] H. Zhang, X. Wen, Y. Wang, J. Solid State Chem. 180 (2007) 1636–1647.
[36] Y. Lei, L. Zhang, G. Meng, G. Li, X. Zhang, C. Liang, W. Chen, S. Wang, Appl. Phys. Lett. 78 (2001) 1125–1127.
[37] G. Liu, J. Shi, F. Zhang, Z. Chen, J. Han, C. Ding, Angew. Chem. Int. Ed. 53 (2014) 7295–7299.
[38] X. Chang, T. Wang, P. Zhang, J. Zhang, A. Li, J. Gong, J. Am. Chem. Soc. 137 (2015) 8356–8359.
[39] F. Francisco, G. Germa, B. Juan, B. Peter, Z. Arie, J. Electrochem. Soc. 150 (2003) 293–298.
[40] K.M. Parida, L. Mohapatra, Chem. Eng. J. 179 (2012) 131–139.
[41] C. Tard, Chem. Rev. 109 (2009) 2245–2274.

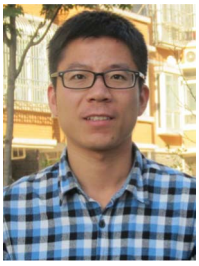

Ruikang Zhang received his Bachelor's degree in 2012 from East China University of Science and Technology. He joined Professor Min Wei's group as a PhD candidate at Beijing University of Chemical Technology in 2013. His research interests currently focus on the design and fabrication of photoelectrodes for water splitting.

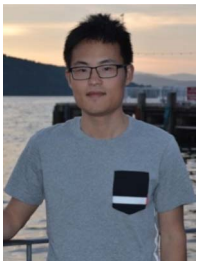

Mingfei Shao received his PhD degree from Beijing University of Chemical Technology in 2014 supervised by Prof. Xue Duan, after which he joined the staff of BUCT. He has been a visiting student in the University of Oxford (in 2013). His current research interests are mainly focused on the controlled synthesis of layered functional materials and their applications in electrochemical and photoelectrochemical energy storage and conversions.

Simin Xu received his Bachelor's degree from Beijing University of Chemical Technology (BUCT) in Applied Chemistry in 2011. He is now a Ph.D. candidate under the supervision of Prof. Xue Duan in the BUCT. His research interests mainly focus on the experimental and computational investigation of the physical and chemical properties of layered double hydroxides.

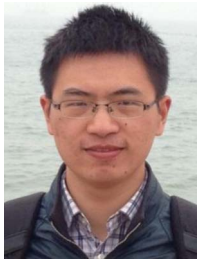

Fanyu Ning received his Bachelor's degree from Beijing University of Chemical Technology (BUCT) in Applied Chemistry in 2011. He is now a Ph.D. candidate under the supervision of Prof. Min Wei in the BUCT. His research interests mainly focus on the design and fabrication of layered double hydroxides nanostructures for energy storage and conversion.

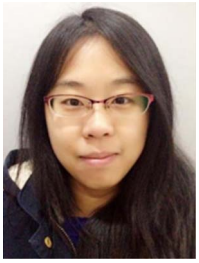

Lei zhou received her Bachelor's degree in 2013 from Beijing University of Chemical Technology. She joined Prof. Xue Duan's group as a PhD candidate at Beijing University of Chemical Technology in 2013. Her research interests currently focus on the design and fabrication of electrodes for small molecules electrocatalysis.

Min Wei obtained her BEng degree in 1995 and MEng degree in 1998 from Beijing University of Chemical Technology (BUCT). She subsequently received her PhD from Peking University in 2001, after which she joined the staff of BUCT. She was promoted to full Professor in 2005. She has been a visiting scholar in the Georgia Institute of Technology (in 2008). Her research interests focus on inorganic-organic composite functional materials as well as new catalysts.